

# Sodium Persulfate Pre-treatment of Copper Foils Enabling Homogenous Growth of Cu(OH)<sub>2</sub> Nanoneedle Films for Electrochemical CO<sub>2</sub> Reduction

Kim Robert Gustavsen, Erik Andrew Johannessen, and Kaiying Wang\*<sup>[a]</sup>

Oxide-derived copper (OD–Cu) catalysts have received widespread attention for their ability to produce energy-dense multicarbon products. Within this class of materials, nanostructured copper hydroxide (Cu(OH)<sub>2</sub>) has shown excellent catalytic properties, but its synthesis requires complex pre-treatment steps of the Cu surface. In this study, we have developed a simple two-step synthesis method for homogenous Cu(OH)<sub>2</sub> nanoneedle films using a sodium persulfate pre-treatment step prior to anodization. The Cu(OH)<sub>2</sub> nanoneedle

films show drastically enhanced uniformity after the pre-treatment due to improved current distribution and can be grown over large surface areas (63 cm<sup>2</sup>). As a catalyst for CO<sub>2</sub> reduction, the Cu(OH)<sub>2</sub> favours ethylene formation, with a near total suppression of methane production. A peak faradaic efficiency (FE) of 36.5% is found at –1.0 V vs. the reversible hydrogen electrode (RHE), and the catalyst remains stable while providing an ethylene to methane ratio of 27.8 after 6 h of reaction.

## Introduction


The electrochemical reduction of CO<sub>2</sub> into higher order organic chemicals and fuels has shown to be a potent green methodology to help reducing our dependence on fossilized fuels. Copper (Cu) has in this respect been extensively investigated in search for a suitable catalyst due to its intrinsic ability to form energy-dense hydrocarbons. The modification of Cu into oxygen-derived Cu (OD–Cu) catalysts has emerged as a prime candidate as it facilitates carbon-carbon (C–C) coupling, leading to significantly higher selectivity for ethylene (C<sub>2</sub>H<sub>4</sub>) production.<sup>[1]</sup> Numerous mechanisms for this enhanced selectivity have been proposed, such as the existence of sub-surface oxides during reaction conditions as well as increased local pH induced by the larger surface roughness on the reduced Cu surface. However, there has been no clear consensus on the exact cause for the improved catalytic activity. The emergence of OD–Cu triggered an incentive to identify in what way the method of oxide growth affects the catalytic properties of Cu. A prime example is the anodization of Cu foils to yield copper hydroxide (Cu(OH)<sub>2</sub>) films with high-aspect-ratio nanoneedle structures. These Cu(OH)<sub>2</sub> nanoneedles shows greater affinity towards the generation of C<sub>2</sub>H<sub>4</sub> at the expense of methane (CH<sub>4</sub>), with stable performance for more than 40 h.<sup>[2]</sup> Recent studies also suggest that local electric fields induced by the

unique nanoneedle morphology play a key role in promoting the C–C coupling.<sup>[3]</sup>

While the effect of anodization parameters on the Cu(OH)<sub>2</sub> film morphology and properties have been extensively studied, the initial condition of the Cu foil surface itself is crucial for achieving a satisfactory film quality. Factors such as surface irregularities and wettability can result in poor current distribution during the anodization process. This may lead to an uneven nanoneedle film in terms of thickness and morphology, which in turn can have detrimental effect on the CO<sub>2</sub> reduction reaction (CO<sub>2</sub>RR) selectivity. Thus, extensive surface treatment procedures have been applied to address these issues, such as mechanical polishing with emery papers<sup>[4]</sup> or alumina powders,<sup>[5]</sup> chemical polishing with HNO<sub>3</sub>,<sup>[6]</sup> electrochemical polishing,<sup>[7]</sup> and chemical treatment using HCl to remove surface oxides.<sup>[4a,8]</sup> Often, a rather complicated process including a combination of polishing and chemical treatment steps must be used to obtain a film quality that is satisfactorily uniform.<sup>[4a,7]</sup>

In this paper, we report a two-step synthesis method for large area Cu(OH)<sub>2</sub> nanoneedle films using a simple sodium persulfate pre-treatment step that increases the wettability of the Cu foils. The sodium persulfate removes crevices and surface contaminants such as carbon and oxygen which in turn reduces the formation of defects such as pinholes. A cleaner surface will permit the current distribution to become more uniform in the subsequent anodization step, allowing the formation of homogenous Cu(OH)<sub>2</sub> nanoneedle films over a large surface area (63 cm<sup>2</sup>). Moreover, investigation of the catalytic properties of the Cu(OH)<sub>2</sub> nanoneedle films reveals a strong preference for C<sub>2</sub>H<sub>4</sub> production over CH<sub>4</sub>, with a substantial increase in current density and catalytic stability compared to the pristine Cu foil catalyst.

[a] K. R. Gustavsen, Prof. Dr. E. A. Johannessen, Prof. Dr. K. Wang  
Department of Microsystems  
University of South-Eastern Norway  
Raveien 205  
3184 Horten, (Norway)  
E-mail: kaiying.wang@usn.no

 © 2022 The Authors. Published by Wiley-VCH GmbH. This is an open access article under the terms of the Creative Commons Attribution Non-Commercial License, which permits use, distribution and reproduction in any medium, provided the original work is properly cited and is not used for commercial purposes.

## Results and Discussion

An illustration of the anodization process and the experimental setup used subsequently for the electrochemical  $\text{CO}_2$  reduction measurements are given in Figure 1. The setup for  $\text{CO}_2$  reduction and quantification of the gaseous reaction products is explained in detail in the Experimental Section. Figure 1a shows the result of the anodization with and without the pre-treatment step. Upon pre-treating the Cu foil with sodium persulfate, the surface becomes brighter in colour. Furthermore, contact angle measurements with water show that the hydro-

philic properties of the surface increases from  $80^\circ$  for the pristine Cu foil to  $14^\circ$  following the pre-treatment, indicating an increase in surface energy.<sup>[9]</sup>

Subsequent measurement repeated for the treated Cu following exposure to ambient air shows that the contact angle gradually increased to  $72^\circ$  after 6 h, suggesting that the surface energy was returning to its original level due to reoxidation. An SEM image of the pristine Cu foil in Figure 2a shows a significant number of crevices of roughly  $10\ \mu\text{m}$  in width. After pre-treatment, most of the crevices have been eliminated while adding a surface roughness at a lower-hierarchy level (Fig-

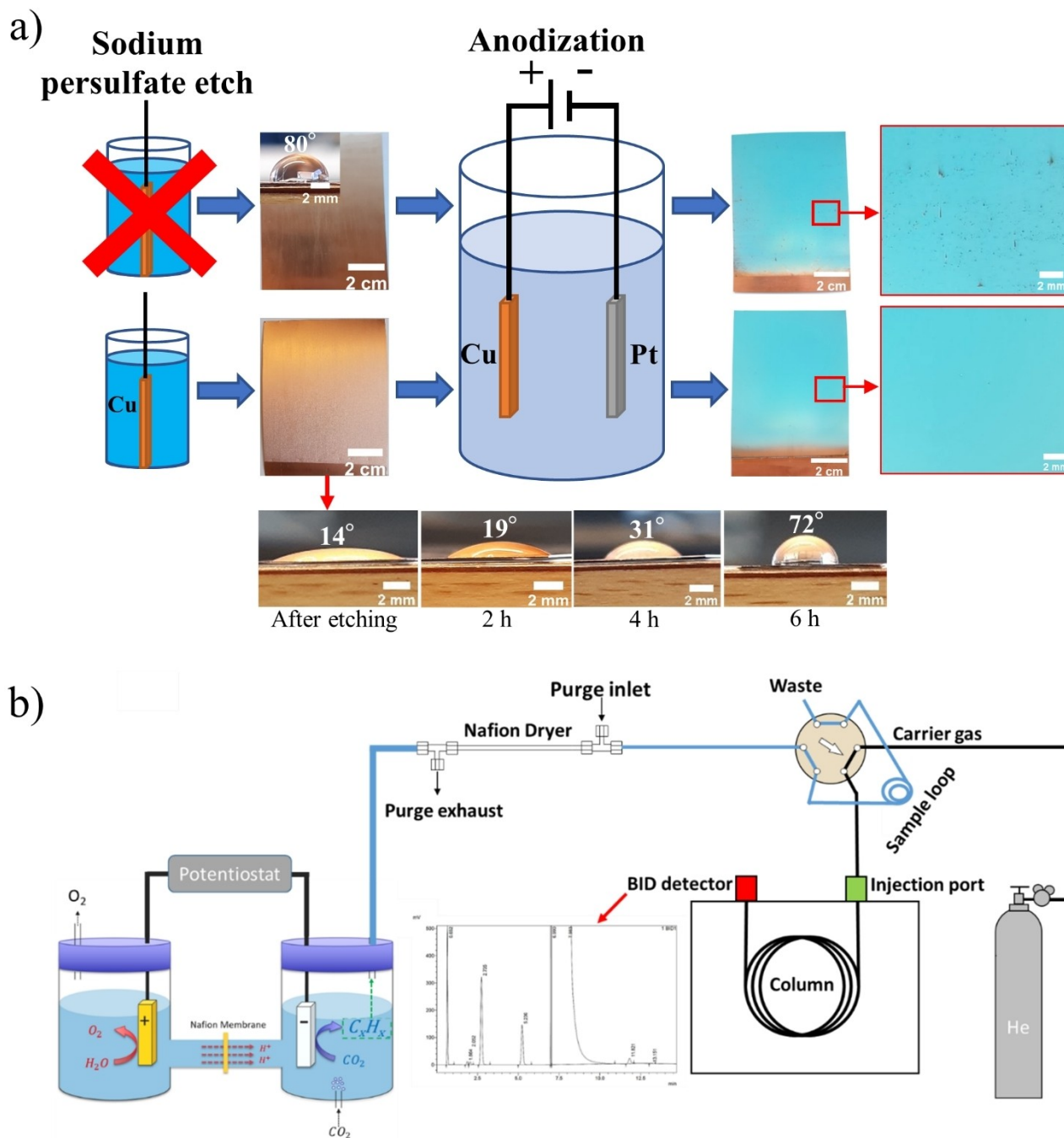


**Figure 1.** a) The process flow illustrating the development of the  $\text{Cu}(\text{OH})_2$  nanoneedle films and b) schematic of the setup used for the electrochemical measurements and gas quantification.

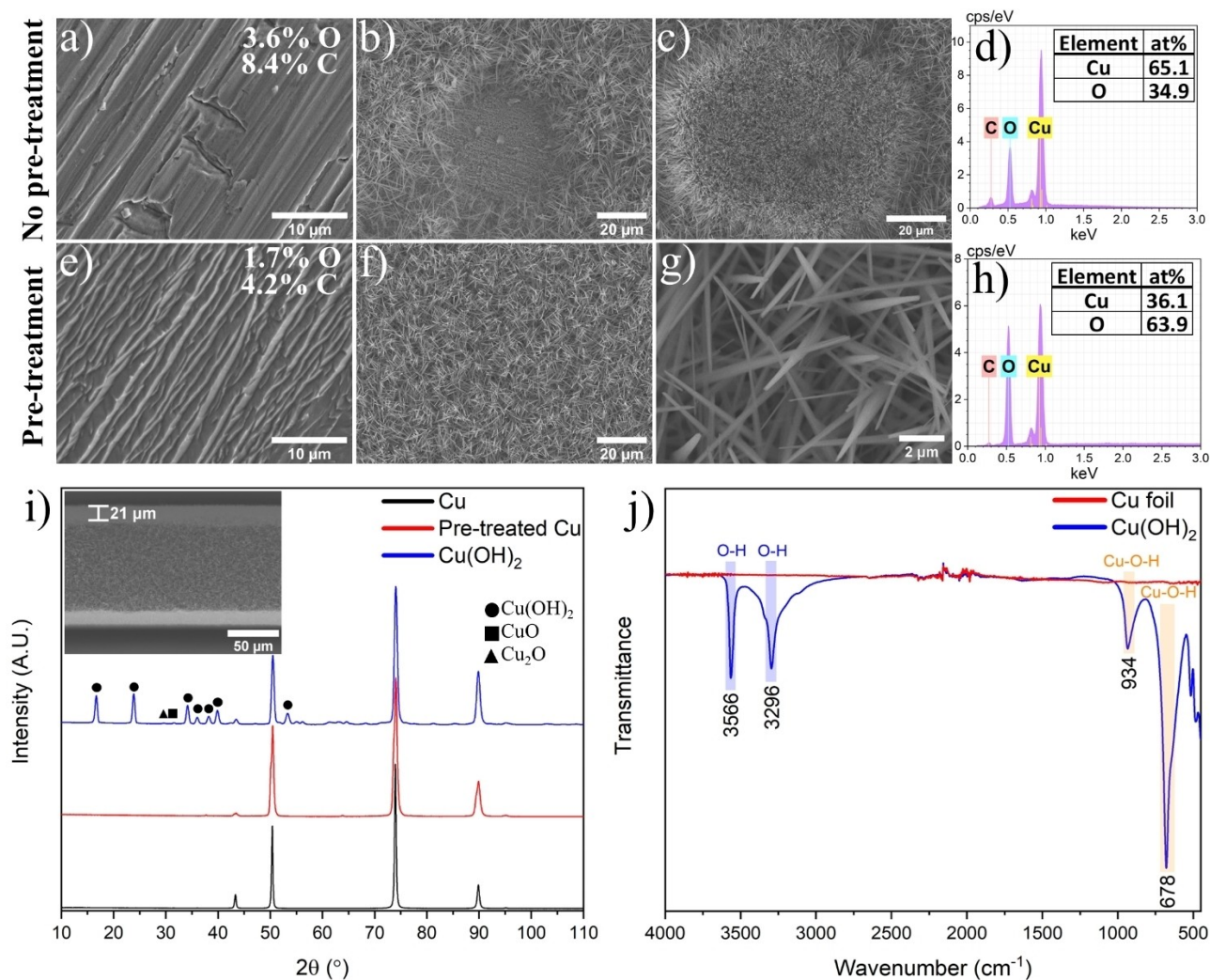


**Figure 2.** SEM images of a) the pristine Cu foil, b) pinhole and c) patch with reduced growth on the anodized surface, and d) EDX spectrum of the layer inside the pinhole observed in c). SEM images of the e) Cu foil after pre-treatment, f)–g) pre-treated Cu sample after anodization, and h) EDX spectrum of the nanoneedles in Figure g). i) XRD spectra of the Cu foil before and after pre-treatment as well as the Cu(OH)<sub>2</sub> film. j) FTIR spectra of the pristine Cu foil and Cu(OH)<sub>2</sub> film.

ure 2e) that increased the effective surface area. Energy Dispersive X-Ray Analysis (EDX) performed before and after pre-treatment shows a reduction in both oxygen and carbon content from 3.6% and 8.4% to 1.7% and 4.2%, respectively.

Anodization of the Cu foils results in a light-blue film as observed in Figure 1a. However, a significant amount of surface defect in form of “black” spots are found when anodizing the pristine Cu foil. On the other hand, anodization of the pre-treated Cu foil leads to a smooth and uniform surface without noticeable surface defects. Further investigation of the black spots in the SEM reveals the growth of nanoneedles surrounding empty areas of 30–50 μm in size as shown in Figure 2b.

The EDX analysis confirms the formation of Cu<sub>2</sub>O layers in these areas (Figure 2d). There are also several patches where the density, shape, and size of nanoneedles vary drastically, indicating a variation in nucleation rate (Figure 2c). In contrast, anodization following the pre-treatment (etching) with sodium persulfate results in a high and even density of nanoneedles

across the whole surface area (Figure 2f). The nanoneedles have an average width close to the needle tip of ~200 nm (Figure 2g), and the film thickness is ~21 μm (Figure 2i, inset). Moreover, EDX measurements of the nanoneedles show an oxygen concentration of 64.5%, roughly a 2:1 ratio of oxygen to copper (Figure 2h). Overall, the pre-treatment leads to a vastly improved uniformity compared to the direct anodization of the pristine sample. Since the surface energy has been reduced back to approximately that of the pristine Cu sample after 6 h, it indicates that it is primarily the removal of carbon and the native oxide layer from the surface rather than an increase in surface area that is responsible for the initial increase in surface energy.

To evaluate the defect mechanism, we first considered the side reactions during anodization. There are two main competing side reactions to the formation of Cu(OH)<sub>2</sub>, namely the formation of CuO through the dehydration of Cu(OH)<sub>2</sub>,<sup>[10]</sup> and the oxidation of Cu to form Cu<sub>2</sub>O.<sup>[11]</sup> As the dehydration of

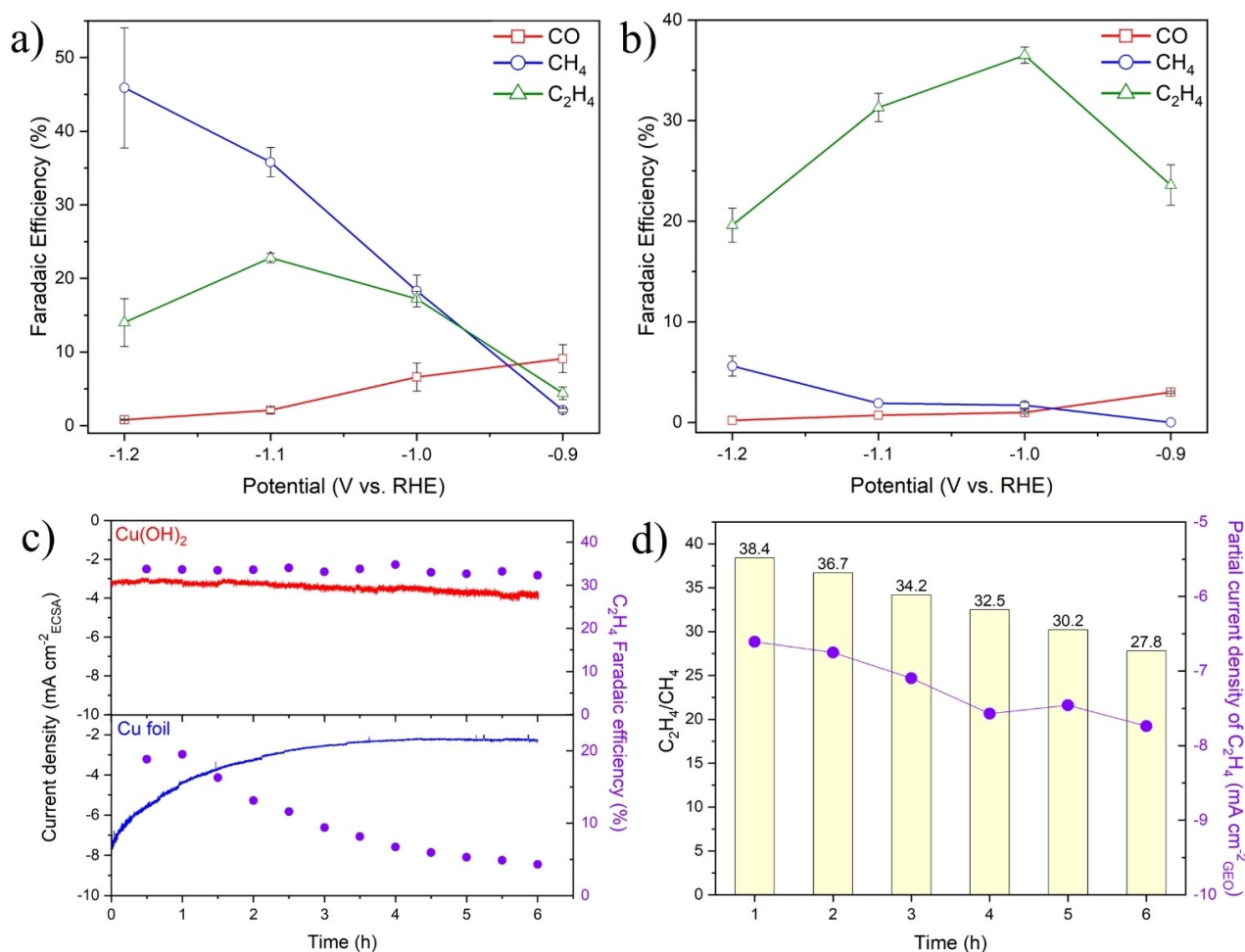
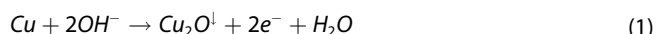


**Figure 3.** Electrochemical characterization: a) selectivity of the Cu foil catalyst, b) selectivity of the Cu(OH)<sub>2</sub> catalyst, c) stability test, and d) the C<sub>2</sub>H<sub>4</sub> to CH<sub>4</sub> production ratio including the partial current density from C<sub>2</sub>H<sub>4</sub> production obtained for the Cu(OH)<sub>2</sub> catalyst during the stability test.

Cu(OH)<sub>2</sub> is a purely chemical reaction, it is more pronounced at higher temperature and KOH concentration. On the other hand, the formation of Cu<sub>2</sub>O arises from the side reaction given in Equation (1).



In general, the formation of both CuO and Cu<sub>2</sub>O can be circumvented by increasing the current density (> 1.0 mA cm<sup>-2</sup>) as they are more favourable at lower current densities.<sup>[10]</sup> In our case, an applied current density of 1.6 mA cm<sup>-2</sup> should be sufficient to avoid these parasitic reactions. While the cracks and crevices will negatively impact the current distribution, they will not result in the type of defects observed in Figures 2b–c, as the sharp edges in these surface irregularities would attract a higher current density, inducing rapid growth of Cu(OH)<sub>2</sub>. Thus, the pinholes occur due to the presence of surface contaminants partially or fully blocking the growth of Cu(OH)<sub>2</sub>. Consequently, there will be areas without growth as shown in Figure 2b, or with a reduction in growth rate as shown in Figure 2c.

The empty sites consist of a Cu<sub>2</sub>O layer, that, according to the EDX measurements, is significantly thicker (~10-fold) than the native oxide layer found on the pristine Cu. Areas with thicker oxide layers on the pristine Cu surface would effectively block or reduce the current at that site during anodization. While a partial blockage can result in a reduced growth rate of the Cu(OH)<sub>2</sub> as shown in Figure 2c, it can also favour side reactions if the current density is reduced sufficiently.

The structure of the Cu(OH)<sub>2</sub> nanoneedle films was analysed by X-ray diffraction (XRD) and Fourier-transform infrared spectroscopy (FTIR). The acquired XRD spectra (Figure 2i) show strong peaks indicative of the orthorhombic copper hydroxide phase with small diffraction peaks associated with Cu<sub>2</sub>O and CuO. The FTIR spectra of the anodized Cu sample and Cu foil reference can be seen in Figure 2j. No peaks were detected for the Cu foil, whereas the Cu(OH)<sub>2</sub> sample displayed four major peaks. The peaks found at 3566 cm<sup>-1</sup> and 3296 cm<sup>-1</sup> are ascribed to the stretching modes of the OH groups. More precisely, the peak at 3566 cm<sup>-1</sup> belongs to the free OH group and the peak at 3296 cm<sup>-1</sup> is due to the hydrogen-bonded OH group.<sup>[12]</sup> Furthermore, the peaks at 934 cm<sup>-1</sup> and 678 cm<sup>-1</sup> arise from the Cu–O–H bonds.<sup>[13]</sup>

The product selectivity of the Cu foil as a function of potential is shown in Figure 3a. Consistent with previous reports, the Cu foil favours the formation of CH<sub>4</sub>. In comparison, the Cu(OH)<sub>2</sub> catalyst effectively suppresses the formation of CH<sub>4</sub> in favour of C<sub>2</sub>H<sub>4</sub> production (Figure 3b). A peak FE(C<sub>2</sub>H<sub>4</sub>) of 36.5% is attained for the Cu(OH)<sub>2</sub> catalyst at a potential of −1.0 V vs. RHE, which is more than double that of the pristine Cu foil operating at the same potential.

Next, we sought to test the stability of the catalysts by performing CO<sub>2</sub>RR for 6 h at −1.0 V vs. RHE. In the stability test, the electrochemically active surface area (ECSA) was used to normalize the current. The roughness factor of the Cu(OH)<sub>2</sub> catalyst was calculated to be 6.17 relative to the pristine Cu, with an ECSA of 2.96 cm<sup>2</sup>. Over the duration of the test, the Cu foil shows a decrease in current density from 8.5 to 2.2 mA cm<sup>−2</sup>, with FE(C<sub>2</sub>H<sub>4</sub>) declining after one hour of operation (Figure 3c). At the end of the 6-hour stability test, the Cu foil displayed a FE(C<sub>2</sub>H<sub>4</sub>) of ~4%, down from an initial FE of ~19%. The decline in FE(C<sub>2</sub>H<sub>4</sub>) was accompanied by a doubling in the FE(H<sub>2</sub>) and FE(CO), showing clear signs of deactivation. On the other hand, the Cu(OH)<sub>2</sub> catalyst showed exceptionally stable C<sub>2</sub>H<sub>4</sub> selectivity. An increase in the current density from 3.3 to 3.9 mA cm<sup>−2</sup>, together with a minor increase in both FE(H<sub>2</sub>) and FE(CH<sub>4</sub>), was observed. The increase in FE(CH<sub>4</sub>) is rather low, from 0.6% at the beginning of the test, to 1.2% after 6 h, whereas the FE(H<sub>2</sub>) increased by ~2%. The increase in CH<sub>4</sub> production, in combination with a drop of ~1% in the FE(C<sub>2</sub>H<sub>4</sub>), results in a slightly lower C<sub>2</sub>H<sub>4</sub> to CH<sub>4</sub> ratio as seen in Figure 3d. After one hour of operation, a C<sub>2</sub>H<sub>4</sub> to CH<sub>4</sub> ratio of 38 is observed, whereas a ratio of 30 is retained after 6 h.

## Conclusion

In summary, a two-step synthesis method for growing homogeneous Cu(OH)<sub>2</sub> nanoneedle films over large surface areas was developed by using a sodium persulfate pre-treatment step prior to anodization. A direct anodization of the pristine Cu foil resulted in low quality Cu(OH)<sub>2</sub> nanoneedle films with several pinholes and patches with uneven growth. In contrast, inclusion of the pre-treatment step aided in the homogenous growth of Cu(OH)<sub>2</sub> without defects by providing a uniform surface roughness through the elimination of crevices, removal of the native oxide layer and carbon on the surface and improving the contact at the interface of the Cu foil and electrolyte due to better wetting as the surface energy had been increased. As a catalyst for CO<sub>2</sub>RR, the Cu(OH)<sub>2</sub> demonstrates a strong preference for C<sub>2</sub>H<sub>4</sub>, reaching a FE(C<sub>2</sub>H<sub>4</sub>) of 36.5% at −1.0 V vs. RHE. Furthermore, a stable formation of C<sub>2</sub>H<sub>4</sub> was obtained for 6 h in which a ratio of C<sub>2</sub>H<sub>4</sub> to CH<sub>4</sub> production of 30:1 was achieved at the end of the 6-hour stability test. In comparison, the pristine Cu foil rapidly declined in terms of both C<sub>2</sub>H<sub>4</sub> selectivity and current density while the hydrogen evolution reaction selectivity doubled.

## Experimental Section

**Catalyst preparation.** The catalyst was made from 0.1 mm thick Cu foils (99.9999%) with a geometrical surface area of 63 cm<sup>2</sup>. The foils were cleaned using acetone and isopropanol and rinsed in deionized water. The Cu foils were then etched in 20% sodium persulfate solution for 5 min and 30 seconds (Step 1), rinsed in deionized water and ethanol before drying with nitrogen. Anodization of the copper foils was immediately performed in a 3 M KOH solution in a Teflon beaker with a Pt mesh acting as a counter electrode (Step 2). A current density of 1.6 mA cm<sup>−2</sup> was applied for 15 min at room temperature. For the electrochemical CO<sub>2</sub> reduction measurements, the Cu(OH)<sub>2</sub> samples were cut into smaller pieces with a geometrical surface area of 0.48 cm<sup>2</sup>, while the Cu foil catalyst had a geometrical surface area of 1 cm<sup>2</sup>.

**Material characterization.** The crystal structure of the catalysts was investigated with low angle X-ray diffraction (XRD) (Thermo Fischer Equinox 1000) using Cu–K $\alpha$  radiation with a wavelength of 1.54 Å. Fourier-transform infrared spectroscopy, FTIR, (Thermo Fischer Nicolet iS50) was used to detect the chemical bonds associated with Cu(OH)<sub>2</sub>. Surface morphologies were observed using a scanning electron microscope (SEM) (Hitachi SU 3500), which was equipped with an electron dispersive x-ray spectroscope (EDX) for elemental analysis.

**Electrochemical measurements.** All electrochemical measurements were performed with a CHI660E electrochemical workstation in a custom glass H-cell (Adams and Chittenden). A Nafion 117 proton exchange membrane separated the anodic and cathodic compartments. The counter and reference electrodes consisted of a coiled Pt wire and Ag/AgCl (3 M KCl), respectively. The cathodic and anodic side were filled with 80 mL of CO<sub>2</sub>-saturated 0.1 M KHCO<sub>3</sub> electrolyte with a measured pH of 6.8. iR compensation was performed by measuring the resistance vs. the open circuit potential and was in the range of 6–14  $\Omega$ . Measurements were conducted for 90 min at each potential, with a fresh catalyst and electrolyte used for each run. All catalysts were pre-conditioned at a potential of −1.1 V vs the reversible hydrogen electrode (RHE) for 300 s prior to the CO<sub>2</sub>RR. The potentials were converted to RHE using Equation (2).

$$E \text{ vs RHE} = E \text{ vs Ag/AgCl}(3 \text{ M KCl}) + 0.209V + 0.05916 \times \text{pH} \quad (2)$$

The roughness factor and ECSA were determined by running cyclic voltammetry (CV) scans at different scan rates in the non-faradaic region of −0.1 to −0.3 V vs. RHE. The double layer capacitance ( $C_{dl}$ ) was calculated from the difference between the cathodic ( $i_c$ ) and anodic ( $i_a$ ) currents peaks divided by the scan rate according to Equation (3). The value obtained from the pristine Cu foil was used as a reference.

$$C_{dl} = \frac{i_c - i_a}{\text{scan rate}} \quad (3)$$

The roughness factor ( $R_f$ ) of the Cu(OH)<sub>2</sub> catalyst was calculated by dividing the  $C_{dl}$  to that of the pristine Cu catalyst. ECSA was obtained from Equation (4), where  $S$  is the geometrical surface area.

$$\text{ECSA} = R_f S \quad (4)$$

**Gas quantification.** The experimental setup is presented in Figure 1b. The quantification of gaseous reaction products was done using a gas chromatograph, GC, (Shimadzu-GC-2010 PLUS) equipped with a ShinCarbon ST column for separation of the gases and a Dielectric-Barrier Discharge Ionization Detector (BID). Helium

(99.9999%) was used as the carrier gas. The H-cell was set up in an on-line configuration with the headspace of the cathodic compartment connected to a 6-port sampling valve equipped with a 0.5 mL sample loop for injection. A Nafion tubing dryer was connected between the cell and the gas-sampling valve to reduce the amount of water vapour present in the gas stream. The calibration curves were made using custom-made gas mixtures containing H<sub>2</sub>, CO, CH<sub>4</sub>, C<sub>2</sub>H<sub>4</sub>, and C<sub>2</sub>H<sub>6</sub> in a CO<sub>2</sub> balance (Nippon Gases). A mass flow controller was used to set the flow rate of CO<sub>2</sub> (20 sccm) being continuously fed into the cell. The content of the sample loop was injected into the GC every 30 min over the duration of the experiments. The Faradaic efficiency (FE) was calculated using the formula in Equation (5), where  $m$  is the number of moles of product derived from the GC measurement,  $n_x$  is the number of electrons required for reduction to product  $x$ ,  $F$  is Faraday's constant (96500 C/mol), and  $Q$  is the charge (in C). In our case, the charge was calculated as the time it takes to fill the sample loop based on the gas flow rate multiplied with the current averaged 30 s prior to injection.

$$FE = \frac{m \times n_x \times F}{Q} \times 100 \quad (5)$$

Prior to the experiments, a silver foil was used as a catalyst for CO<sub>2</sub>RR to ensure that the setup was working properly. Silver foil is known to produce only H<sub>2</sub> and CO, meaning that the FE should be close to 100%. A total FE of 98.1% was attained for the silver catalyst at a potential of  $-1.1$  V vs RHE.

## Acknowledgements

The authors acknowledge support from the research grants GRAFTID (project #RO-NO-2019-0616 from EEA (European Economic Area)-Norway-Romania), EEA-Poland NOR/POLNORCCS/PhotoRed/0007/2019-00, and the Research Council of Norway projects #314012 and #295864.

## Conflict of Interest

The authors declare no conflict of interest.

## Data Availability Statement

The data that support the findings of this study are available from the corresponding author upon reasonable request.

**Keywords:** anodization · copper hydroxide · electrochemical CO<sub>2</sub> reduction · multicarbon reaction products · nanoneedles

- [1] K. R. Gustavsen, K. Wang, *Phys. Chem. Chem. Phys.* **2021**, *23*, 12514–12532.
- [2] G. Iijima, T. Inomata, H. Yamaguchi, M. Ito, H. Masuda, *ACS Catal.* **2019**, *9*, 6305–6319.
- [3] Y. Zhou, Y. Liang, J. Fu, K. Liu, Q. Chen, X. Wang, H. Li, L. Zhu, J. Hu, H. Pan, M. Miyauchi, L. Jiang, E. Cortés, M. Liu, *Nano Lett.* **2022**, *22*, 1963–1970.
- [4] a) F. Xiao, S. Yuan, B. Liang, G. Li, S. O. Pehkonen, T. Zhang, *J. Mater. Chem. A* **2015**, *3*, 4374–4388; b) T. G. S. Babu, T. Ramachandran, *Electrochim. Acta* **2010**, *55*, 1612–1618.
- [5] a) L. Shoostari, R. Mohammadpour, A. I. Zad, *Mater. Lett.* **2016**, *163*, 81–84; b) N. K. Allam, C. A. Grimes, *Mater. Lett.* **2011**, *65*, 1949–1955.
- [6] L. Arurault, M. H. Belghith, R. S. Bes, *J. Mater. Sci.* **2007**, *42*, 1190–1195.
- [7] W. J. Stepniowski, S. Stojadinović, R. Vasilčić, N. Tadić, K. Karczewski, S. T. Abrahams, J. G. Buijnsters, J. M. C. Mol, *Mater. Lett.* **2017**, *198*, 89–92.
- [8] D. S. Zimbovskiy, A. I. Gavrillov, B. R. Churagulov, *Iop. Conf. Ser. Mater. Sci. Eng.* **2018**, *347*, 012010.
- [9] G. Liu, K. Du, K. Wang, *Appl. Surf. Sci.* **2016**, *388*, 313–320.
- [10] X. Wu, H. Bai, J. Zhang, F. e Chen, G. Shi, *J. Phys. Chem. B* **2005**, *109*, 22836–22842.
- [11] a) D. Reyter, M. Odziemkowski, D. Bélanger, L. Roué, *J. Electrochem. Soc.* **2007**, *154*, K36; b) Y. Deng, A. D. Handoko, Y. Du, S. Xi, B. S. Yeo, *ACS Catal.* **2016**, *6*, 2473–2481.
- [12] A. M. Awwad, B. Albiss, *Adv. Mater. Lett.* **2015**, *6*, 51–54.
- [13] C. Henrist, K. Traina, C. Hubert, G. Toussaint, A. Rulmont, R. Cloots, *J. Cryst. Growth* **2003**, *254*, 176–187.

Manuscript received: June 10, 2022  
Revised manuscript received: August 29, 2022